Review

Molecular imaging: Bridging the gap between neuroradiology and neurohistology

S. Heckl[1], R. Pipkorn[2], T. Nägele[1], U. Vogel[3], W. Küker[1] and K. Voigt[1]

[1]Department of Neuroradiology, University of Tübingen, Medical School, Germany, [2]Central Section of Peptide Synthesis, German Cancer Research Center Heidelberg, Germany and [3]Department of Pathology, University of Tübingen, Medical School, Germany

Summary. Historically, in vivo imaging methods have largely relied on imaging gross anatomy. More recently it has become possible to depict biological processes at the cellular and molecular level. These new research methods use magnetic resonance imaging (MRI), positron emission tomography (PET), near-infrared optical imaging, scintigraphy, and autoradiography in vivo and in vitro. Of primary interest is the development of methods using MRI and PET with which the progress of gene therapy in glioblastoma (herpes simplex virus–thymidine kinase) and Parkinson's disease can be monitored and graphically displayed.

The distribution of serotonin receptors in the human brain and the duration of serotonin- receptor antagonist binding can be assessed by PET. With PET, it is possible to localize neurofibrillary tangles (NFTs) and ß-amyloid senile plaques (APs) in the brains of living Alzheimer disease (AD) patients. MR tracking of transplanted oligodendrocyte progenitors is feasible for determining the extent of remyelinization in myelin-deficient rats. Stroke therapy in adult rats with subventricular zone cells can be monitored by MRI. Transgene expression (ß-galactosidase, tyrosinase, engineered transferrin receptor) can also be visualized using MRI. Macrophages can be marked with certain iron-containing contrast agents which, through accumulation at the margins of glioblastomas, ameliorate the visual demarcation in MRI.

The use of near-infrared optical imaging techniques to visualize matrix-metalloproteinases and cathepsin B can improve the assessment of tumor aggressiveness and angiogenesis-inhibitory therapy. Apoptosis could be detected using near-infrared optical imaging representation of caspase 3 activity and annexin B.

This review demonstrates the need for neurohistological research if further progress is to be made in the emerging but burgeoning field of molecular imaging.

Introduction

By *molecular imaging* we mean the visual representation of biological processes at the cellular and molecular level, mostly with the help of gene expression. In contradistinction to "classical" diagnostic imaging, it aims to probe the molecular abnormalities that are the basis of disease rather than imaging the end-effects of these molecular alterations.

At present, molecular imaging is still basically in the experimental phase; however, it has made a partial debut into clinical medicine. Five already-established methods are used in molecular imaging: MRI, PET, near-infrared optical imaging, scintigraphy, and autoradiography (Fig. 1).

Presently, molecular imaging is mainly used for experimental studies in cells and animals. Using PET, for example, the success of gene therapy in rats and monkeys, but also in humans can be monitored and also assessed. With PET, it is also possible to localize NFTs and APs in the brains of living AD patients.

The distribution of serotonin receptors in the human brain and the duration of the serotonin-receptor antagonist binding can be assessed with PET. Through the visual respresentation of specific parameters of angiogenesis, tumor and metastasis aggressiveness or the success of angiogenesis inhibition in tumor therapy can be determined.

The margins of glioblastomas can be localized through macrophages or lymphocytes, which migrate towards the tumor. Additionally, with MR tracking of transplanted oligodendrocyte progenitors the extent of remyelinization can be determined in myelin-deficient

Offprint requests to: Stefan Heckl, MD, Department of Neuroradiology, University of Tübingen, Medical School, Hoppe-Seyler-Str. 3, 72076 Tübingen, Germany. Fax: 07071-29-5638. e-mail: stefan.heckl@ med.uni-tuebingen.de

rats.

Stroke therapy with subventricular zone cells can be monitored in adult rats. It is also possible to visualize transgene expression (beta-galactosidase, tyrosinase, human engineered transferrin receptor) using MRI.

Tumors can also be visualized via certain receptors (for example, somatostatin receptors in neuroendocrine tumors) through radioactively labeled ligands. Here, a number of aspects of molecular imaging that are relevant for the future of neurohistology are discussed.

Magnetic resonance imaging

MRI uses radiowaves in the presence of a magnetic field to extract information from certain atomic nuclei (most commonly hydrogen). It is primarily used for producing anatomical images, but also gives information on the physicochemical state of tissues, flow, diffusion, motion, and, more recently, molecular targets. MRI is about 10^4-10^6 times less senstive than PET in imaging certain substances. However, MRI is more readily available and the localization is significantly better. The following possibilities arise for molecular imaging with MRI:
1. Visualization of transgene expression.
2. Tracking of oligodendrocyte progenitors in the spinal cord.
3. Monitoring of stroke therapy with subventricular zone cells.

4. Targeting of Alzheimer's amyloid plaques.
5. Localizing tumor margins.
6. Cell nucleus-specific molecular imaging

1. Visualization of transgene expression

Up to now the expression of the following genes could be detected: a.) LacZ gene; b.) tyrosinase gene; c.) human engineered transferrin receptor gene.

a) ß-Galactosidase Gene (LacZ-Gene)

The LacZ gene encodes ß-galactosidase. To be able to visualize ß-galactosidase by MRI Louie et al. (2000) developed a special gadolinium preparation which does not initially induce any changes in MR signal intensity directly after microinjection into the cells of living xenopus laevis embryos (two-cell stage).

Indeed, water access to the first coordination sphere of Gd^{3+} was blocked with a substrate that could be removed by enzymatic cleavage. Once cleavage has occured, Gd^{3+} can interact directly with water protons to increase the MR signal intensity in a T1-weighted image. Galactopyranose was used as a blocking group, which in turn made it possible to measure the activity of galactosidase in the cytoplasm.

The change in signal intensity on MRI can also be produced in vitro (b) and in animal experiments (c) by increasing the iron level in the specific tissue (signal

I. *MRI*	II. *PET*	III. *Optical imaging*	IV. *Scinti-graphy*	V. *Autoradiography*
- ß-galactosidase	- acetylcholine receptor	- somatostatin receptor	- phosphatidylserine	- benzodiazepine receptor
- tyrosinase	- sigma (1) receptor	- phosphatidylserine	- sigma (1) receptor	- acetylcholine receptor
- *E*TfR	- benzodiazepine receptor	- VIP-receptor	- estrogen receptor	- adrenoceptor
- folate receptor	- opioid receptor	- transferrin	- cholecystokinin receptor	- cholecystokinin receptor
- benzodiazepine receptor	- NMDA receptor	- albumin	- somatostatin receptor	- EGFR
- amyloid plaques	- estrogen receptor	- matrix metalloproteinases	- bombesin receptor	- VEGFR
- asialoglycoprotein	- cholecystokinin receptor	- cathepsin B, D	- asialoglycoprotein	- adenosine
- Her-2/neu receptor	- EGFR	- caspase 3	- EGFR	- opioid receptor
- GRP (Bombesin)	- adrenoceptor	- thrombin (serinase)	- VEGFR	- TGF-Beta (endoglin)
- integrin alpha v beta 3	- dopamin receptor 1, 2	- folate receptor	- folate receptor	- sigma 1 receptor
- phosphatidylserine	- 5HT2-serotonin receptor		- adenosine receptor	- neurokinin-1 receptor
- c-myc oncogene (mRNA)	- adenosine receptor		- VIP-receptor	(Substance P)
- cell nucleus	- VEGFR		- melanin	- acetylcholinesterase
	- HSV-thymidine kinase		- dopamin	- fibrin
	- decarboxylase		- NaI-symporter	- Abeta amyloid plaques
	- CEA		- Substance P (NK)	- integrin alpha v beta 3
	- Substance P (NK)		- PSA	- luciferase (mRNA)
	- prostate specific antigene		- CEA	- hmdr1 gene (mRNA)
	- phosphatidylserine		- topoisomerase	- Huntington`s disease gene
	- P-glycoprotein		- endostatin receptor	(mRNA)
	- neurotensin receptor		- phosphatidylserine	
	- integrin alpha v beta 3		- c-erbB-2 (mRNA)	
	- neurofibrillary tangles (NFTs)		- p21(WAF-1/CIP-1)(mRNA)	
	- beta-amyloid senile plaques (APs)		- glycoprotein IIb/IIIa-receptor	
	- acetylcholinesterase		- alpha (v) beta (3) integrin	
	- ß-Galactosidase			
	- hexokinase			
	- GFAP (mRNA)			
	- cytosine deaminase			

Fig. 1. Molecular targets and methods used for molecular imaging.
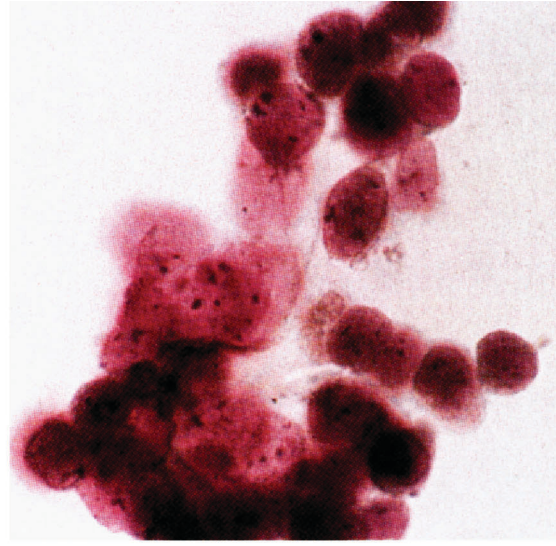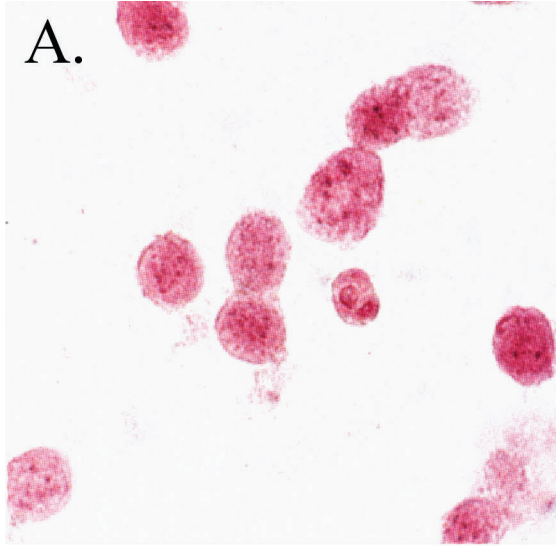
Fig. 2. A. Human embryonal kidney 293 cells transfected with pcDNAtyr (right) and non-transfected cells (left) stained with the Fontana stain for melanin. Note the brownish color and granules in the transfected cells (right), which represent induced melanin, and the absence of those in non-transfected cells (left). **B.** T_1-*weighted MR images* of human embryonal kidney 293 cells embedded in agarose. Cells were transfected with pcDNAtyr (right) or were mock transfected 3 days before MR imaging (left) and then grown in iron-containing cell-culture medium. The higher signal-intensity of cells after gene transfer is due to the overexpression of tyrosinase-producing melanin which scavenges iron. **C.** *Scintigram* of L929 mouse fibroblast cells transfected with pcDNA3tyr (right) (high In-111 binding capacity) and mock transfected cells (left) after incubation with In-111 (trivalent metal ions). Modified from Weisslender et al., 1997.
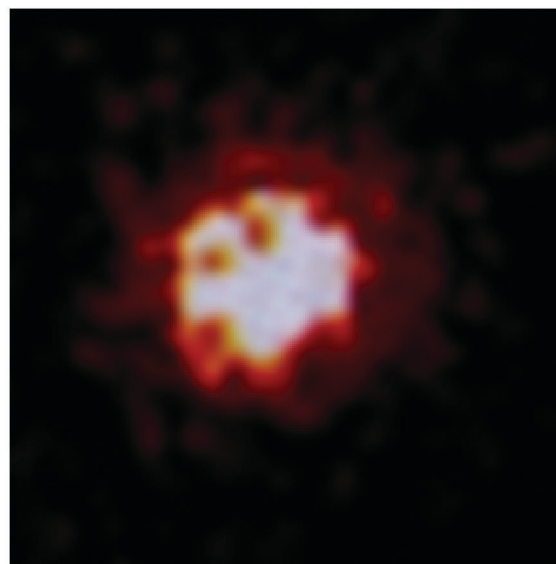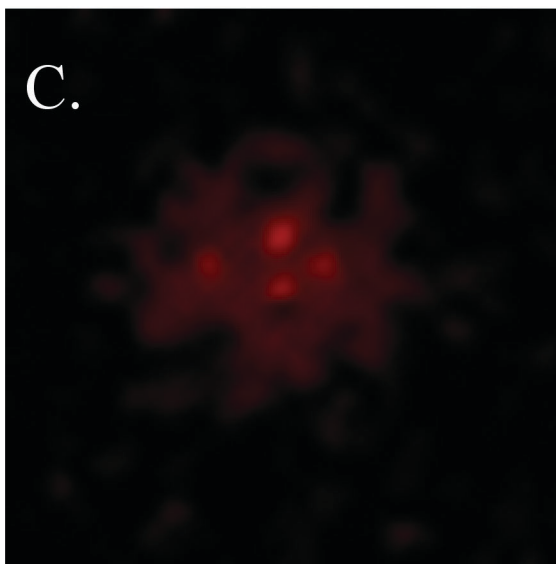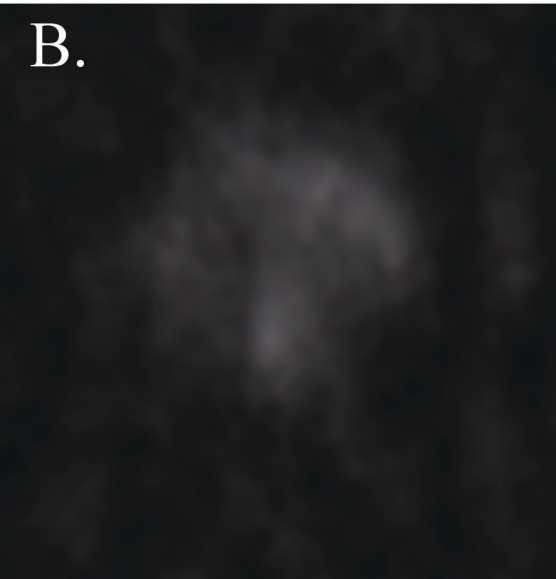
intensity decrease on T2-weighted images) (Figs. 2, 3).

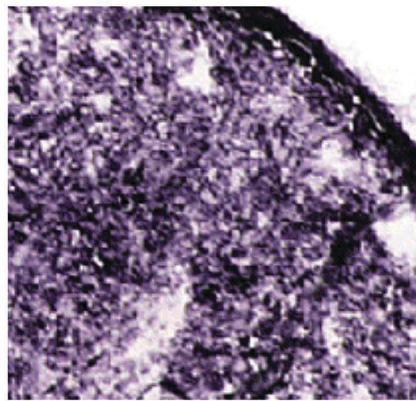b) Increasing intracellular iron concentration through the tyrosinase gene

The concentration of intracellular iron can be increased through transfection of the cell with the tyrosinase gene. When tyrosinase is increased, melanin is produced, which in turn binds iron (iron scavenger) (Enochs et al., 1997; Weissleder et al., 1997) (Fig. 2).

c) Increasing intracellular iron concentration via the gene of the human engineered transferrin receptor

Weissleder et al. (2000) used a human engineered transferrin receptor (ETfR) that lacks the iron-regulatory region and mRNA destabilization motifs in the 3' untranslated region. This results in high levels of the receptor protein at the cell surface and in a 500% increase in holo-transferrin bound by stably transfected cells (Fig. 3). Micro iron oxide nanoparticles (MIONs) (Shen et al., 1993; Högemann et al., 2000, 2002) (Fig. 4) served as the contrast agent. The MIONs were sterically protected by a layer of low-molecular weight dextran to which human holo-transferrin (Tf) was covalently conjugated (Tf-MION). There was a strong correlation between MR signal intensity (decrease in signal intensity on T2-weighted images) and intracellular Tf-MION concentrations, depending on the different levels of mRNA expression of ETfR (Fig. 3).
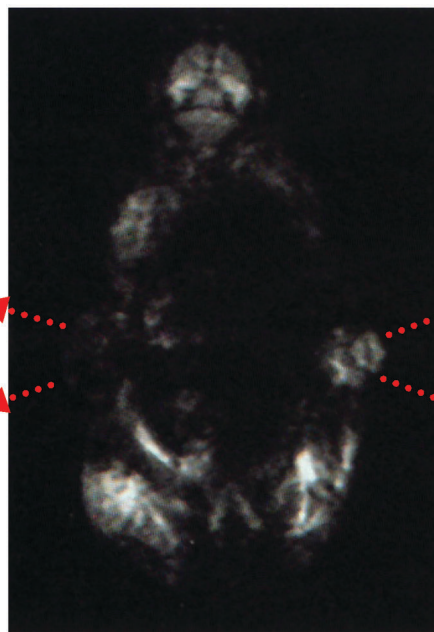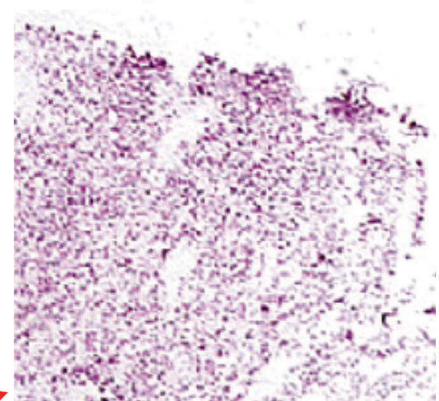
ETfR *positive* gliosarcoma

ETfR *negative* gliosarcoma
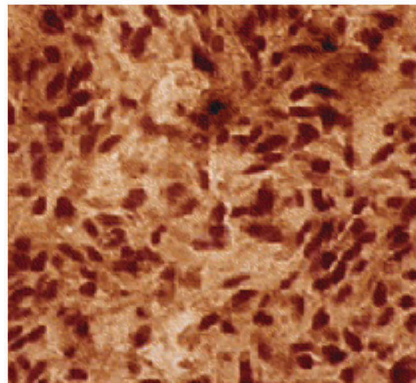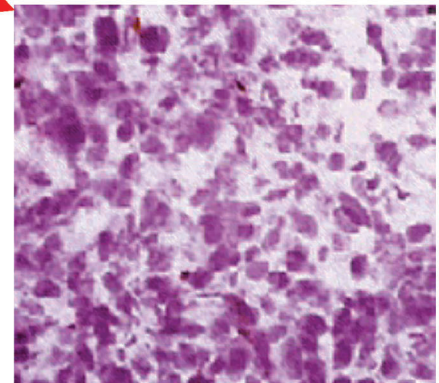

ETfR-Staining

T2-weighted MR image

MION-Staining

ETfR-Staining

MION-Staining

Fig. 3. Middle: In vivo T2-weighted gradient-echo image of a mouse with ETfR+ (left) and *ETfR-* (right) flank 9L gliosarcomas. There are substantial differences between ETR+ and ETR- after intracellular accumulation of the Tf-MIONs. **Top left:** TfR staining of the ETfR+ 9L gliosarcoma (secondary alkaline phosphatase antibody). x 150. **Top right.** TfR staining of the ETfR-, wild-type 9L gliosarcoma from the same mouse (secondary alkaline phosphatase antibody). x 150. **Bottom left:** Iron staining of ETfR+ 9L gliosarcoma from the same mouse (secondary alkaline phosphatase antibody). x 150. **Bottom left:** Iron staining of ETfR+ 9L gliosarcoma 24 hours after intravenous injection of Tf-MION. The iron core of MION is stained with a modified DAB Perl´s stain in which the reaction product is brown. **Bottom right:** Modified DAB Perl´s stain of ETfR- 9L gliosarcoma. Modified from Weissleder et al., 2000.

ETfR gene expression correlates with expression of therapeutic genes when the ETfR gene and the therapeutic genes are contained within the same amplicon. Therefore MRI of ETfR expression (signal intensity decrease on T2-weighted images) can serve as a surrogate for measuring therapeutic transgene expression (Ichikawa et al., 2002).

2. Tracking of oligodendrocyte progenitors in the spinal cord

Bulte et al. (1999) intracellularly labeled oligodendrocyte progenitors (CG-4 cells) ferromagnetically with MION-46 L and grafted them into the spinal cord of neonatal myelin-deficient rats. It was thought that with this method the extent of myelination should be able to be determined. Indeed, an excellent agreement between the areas of decrease in MR contrast enhancement (T2-weighted images) and histopathological staining for iron and newly formed myelin could be observed (Fig. 5A).

Bulte et al. (2003) also tracked magnetically labeled neurospheres transplanted into the ventricles of rats with acute experimental allergic encephalomyelitis (EAE).

3. Monitoring of stroke therapy with subventricular zone cells

Grafted adult subventricular zone (SVZ) cells which were labeled intracellularly with ferromagnetic particles selectively migrated toward ischemic boundary regions in adult rats which had suffered stroke (Zhang et al., 2003). The transplantation significantly enhanced functional recovery when SVZ cells were intracisternally transplanted 48 hours after stroke. Using MRI, the migration could be tracked dynamically (Fig. 5B). The nerve cells were well integrated in their microenvironment with well-formed axosomatic synaptic junctions.

4. Targeting of amyloid plaques in Alzheimer's disease

Visualization of individual ß-amyloid plaques as areas of decreased signal intensity in T2-weighted MR images (ß-amyloid plaques contain elevated levels of metal ions, particularly iron) has been reported in postmortem human tissue specimens (Lovell et al., 1998; Benveniste et al., 1999).

However endogenous iron contained in the hemoglobin of blood in blood vessels and microhemorrhages would create interfering artifacts. Focal areas of decreased signal intensity in T2-weighted MR images (accelerated T2 relaxation) are also present in brain MRIs of healthy individuals as well as in many pathological conditions and are not specific for ß-amyloid plaques.

Therefore, Poduslo et al. (2002) developed a target-specific gadolinium contrast agent called putrescine-gadolinium-amyloid-ß peptide. The transport across the blood-brain barrier following intravenous injection was conferred by a polyamine moiety and the binding to amyloid plaques with molecular specificity by putrescine-amyloid-ß. The probe was injected into transgenic mice with amyloid plaques and mice with normal brains. The mice were killed 4 hours after injection. Each brain was removed and embedded in
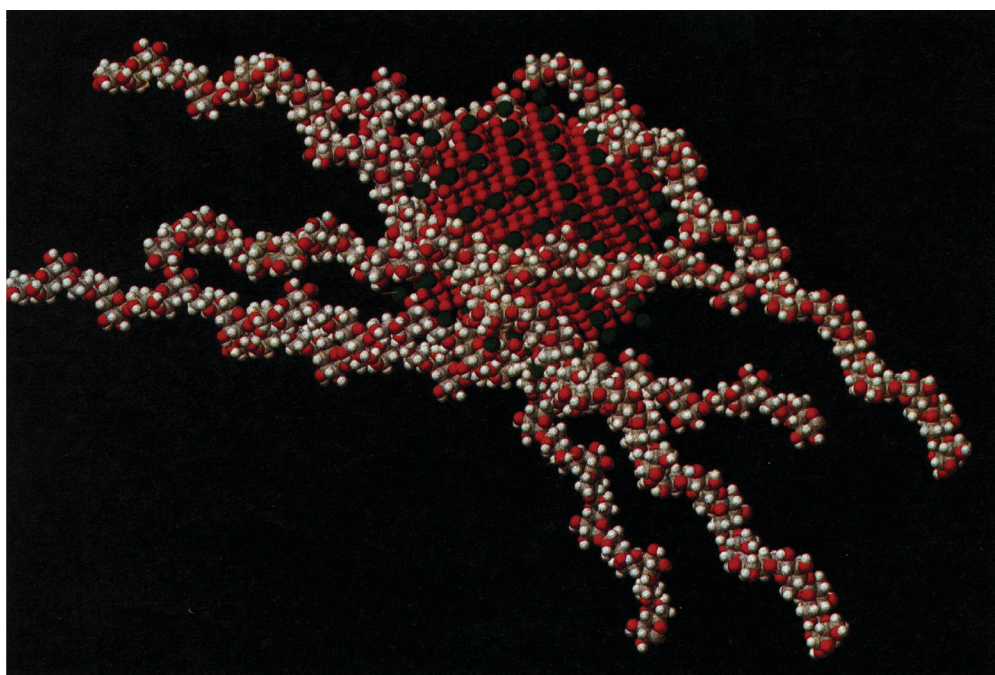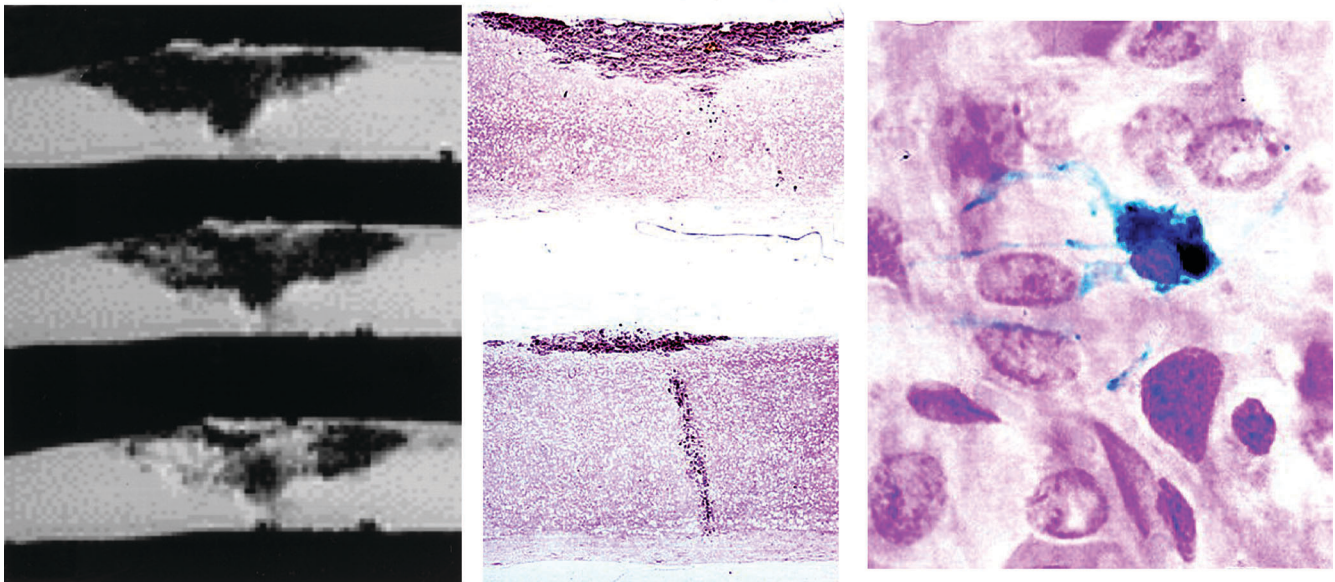

Fig. 4. MION (Micro Iron Oxide Nanoparticles). A low-molecular-weight dextrane capsule contains 2,064 Fe molecules per 3 nm particle core. Adapted from Shen et al., 1993.

A.

B.

before transplantation *day of* transplantation *three days* later *four days* later
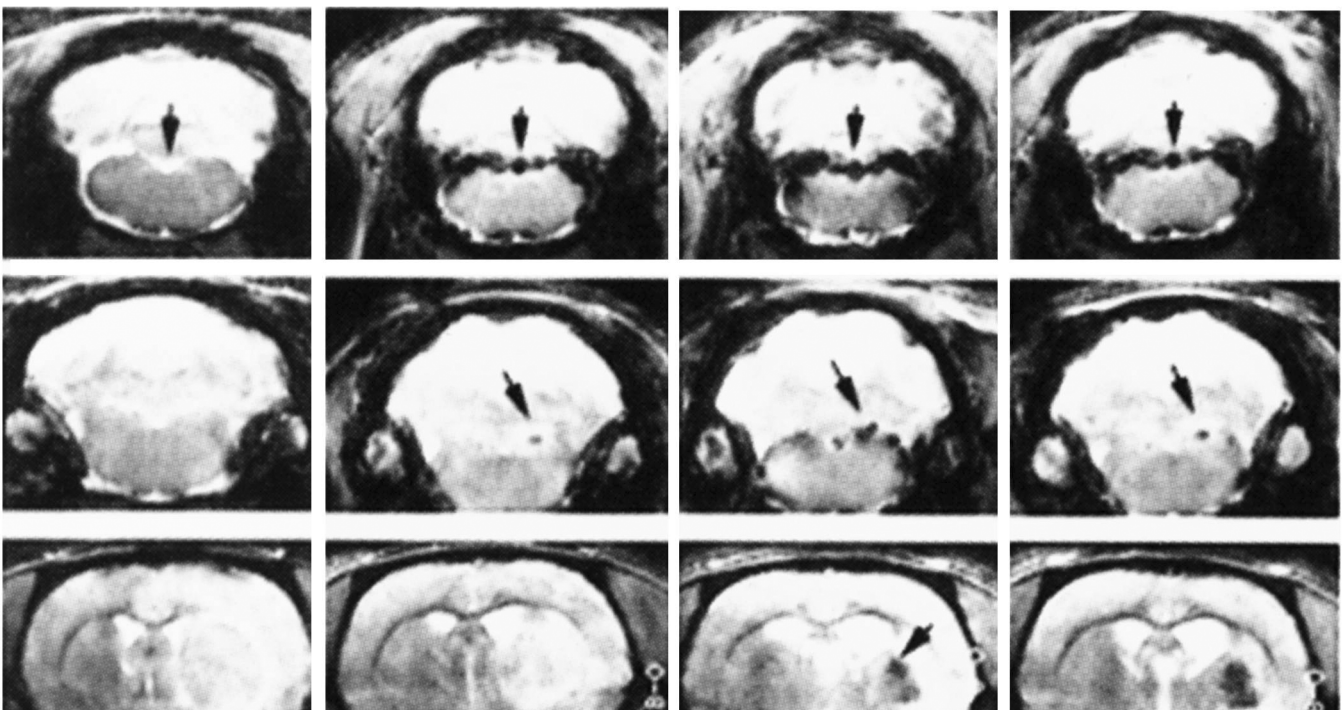

Fig. 5. A. *Myelin-deficient* rat 14 days after transplantation of oligodendrocyte progenitor cells. Left: Sagittal MRI plane. Migration of oligodendrocyte progenitor cells over a distance of 8.4 mm. Middle: Antiproteolipid protein immunolabeling: MRI contrast corresponds closely to the myelination. Note the injection track with cell migration toward the dorsal column. Right: Prussian blue-positive cells in the area of new myelination resemble the cellular morphology of oligodendrocytes. Modified from Bulte et al., 1999. **B.** Migration of intracisternally-transplanted SVZ cells towards the ischemic parenchyma (left hemisphere). The three different rows represent different levels of coronal sections. Modified from Zhang et al., 2003

agar in a glass tube. Using a 7-Tesla MR spectrometer, T2- and T1-weighted images were acquired at very high resolution. After imaging the brains were stained for pathological examination. In transgenic mice a strong correlation between plaques identified on histology (thioflavin S staining, confocal laser scanning microscopy) and focal areas of accelerated T2 and T1 relaxation (visible as dark and bright spots, respectively) was found. The next step in this area of study will be to replicate the findings in live mice.

5. Localizing tumor margins

Glioblastomas contain numerous macrophages, which characteristically lie in the marginal areas of the tumor. Macrophages are situated partly as activated microglial cells in the CNS, but also migrate from the blood. They only take up a very restricted amount of iron. If the iron in the form of MION (Figure 4) is then injected into the rats intravenously, it is phagocytosed by the macrophages.

Because they are mostly situated at the margins of the tumor, on MRI the area between the tumor and the healthy tissue can be visualized because of the increased iron levels (Fleige et al., 2001).

In the future this could help neurosurgeons to remove tumors with a higher degree of certainty that there is no residual tumor (for example, intraoperative MRI examinations).

The tumor margin would be visualized more clearly with an intracellular iron contrast agent than with the gadolinium-complex used in humans up to now, which is only found outside the cell. Surgery causes a more diffuse distribution of the gadolinium-complex and the borders are not at all sharp on intraoperative MRI.

It is also possible to fill other non-iron phagocytosing cells with iron using MION, for example, lymphocytes. The MION is bound to a membrane translocation signal protein (HIV-tat) and taken up in every cell via the cell membrane (Josephson et al., 1999, Lewin et al., 2000). The cells have to be incubated in a MION-containing liquid beforehand, however.

6. Cell nucleus-specific molecular imaging

A transport peptide (a similar peptide sequence to that of the homeodomain of antennapedia) was cleavably and covalently linked to the nuclear localization

Fig. 6. Modular construction of the cell nucleus-directed gadolinium contrast agent: transport petide unit (green)-adress peptide (NLS) (light brown)-gadolinium (magenta) (own photograph).

sequence of SV40 T-antigen via a disulfide bond. The NLS was, in turn, non-cleavably linked to the gadolinium complex via a lysine spacer (Fig. 6). After cleavage of the disulfide bond by disulfide reductases beneath the cell membrane, the NLS becomes the terminal part of the conjugate and can be recognized by the cytoplasmic receptor importin alpha. After binding of the complex to a second cytoplasmic receptor (importin beta), the entire complex of gadolinium-NLS-importin alpha-importin beta is delivered to the nucleus. For nuclear transport an active RAN-GDP system is used. The conjugate has been termed CNN-Gd3+ (Heckl et al., 2002).

Positron emission tomography (PET)

PET is a tomographic imaging technique that detects nuclides by positron emission as they decay. PET shows a very high sensitivity (10^{-10}-10^{-12} molar concentration of the radioactive substrate can be visualized and directly quantified). The resolution, however, is notably worse than with MRI.

With PET it is possible to monitor gene therapy of glioblastoma and Parkinson's syndrome. The serotonin receptor density can be monitored in the brain. Early diagnosis of AD and the visualization of mRNA expression of glial fibrillary acidic protein (GFAP) are also possible using the antisense strategy.

Monitoring glioblastoma therapy using herpes simplex virus thymidine kinase (HSV-tk)

In HSV 1-tk therapy the residual tumor is subjected to multiple injections with retrovirus-producing mouse fibroblasts that contain the virus with the suicide gene (HSV-tk) during surgery. This leads to a continuous release of the virus into the tumor parenchyma.

However, only the mitotically active tumor cells are infected by the retrovirus, not the resting cells. If nontoxic, nonphosphorylated ganciclovir is then administered intravenously it reaches the tumor cell, where it is reconstructed by the HSV-thymidine kinase into a toxic Ganciclovir-phosphate.

The human thymidine kinase found in every cell cannot phosphorylate Ganciclovir.

Via the DNA protein kinases Ganciclovir is phosphorylated further into Ganciclovir-3-phosphate, which blocks the DNA polymerase. This is mainly active in tumor cells, so that Ganciclovir-3-phosphate toxicity develops only insignificantly in the resting cells with low DNA polymerase activity (spontaneous repair of DNA damage).

Since sufficient transfection of the tumor with the HSV-tk gene is only possible to a varying extent (sometimes only 5%), a visual representation of HSV-thymidine kinase is necessary. That way one can test whether the glioblastoma cells in the individual patient have even been reached .

PET provides this information not only in animal experiments (Hospers et al., 2000) (Fig. 7A) but also in
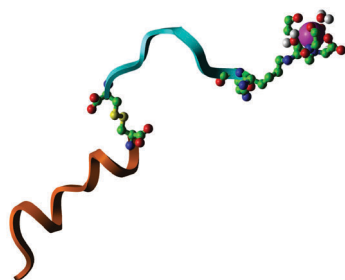
humans (Jacobs et al., 2001) (Fig. 7B). Instead of the normal Ganciclovir, radiolabeled Ganciclovir is administered (^{124}I or ^{18}F, positron emitters) intravenously (other substrates for HSV-tk: [^{18}F] FHPG or [^{124}I] FIAU, Fig. 7A,B).

The radiolabeled Ganciclovir within the glioblastoma cells pretransfected with the HSV-tk gene is phosphorylated by the herpes simplex virus thymidine kinase and becomes toxic.

Phosphorylated Ganciclovir cannot be transported out of the cell by multi-drug-resistant proteins (e.g., MRP 4) of the cell membrane, in contrast to nonphosphorylated Ganciclovir which remains untoxic and will leave the cell (Adachi et al., 2002). The amount of radioactivity retained in the cell is thus also a measure of intracellular herpes simplex virus thymidine kinase activity and therefore of the transfection rate of the tumor with the HSV-tk gene (Fig. 7A,B).

Via gap junctions, however, small amounts of toxic Ganciclovir-3-phosphate can reach the surrounding healthy cells and cause undesired damage (bystander-effect) (Nicholas et al, 2003).

Unfortunately, none of the clinical studies to date dealing with gene therapy of glioblastomas with HSV-thymidine kinase have revealed a significant increase in survival (Rainov, 2000), whereas the results of animal experiments have been very promising.

PET Imaging of presynaptic synthesis of dopamine and postsynaptic D2- receptors

MRI does not show any structural abnormalities in patients with mild Parkinson's disease. However, PET imaging studies show mild abnormalities of increased glucose metabolism in the putamen caused by loss of regulated function in the dopaminergic neurotransmitter pathway. The change in metabolism is modest because only 15% of neurons in the putamen are dopaminergic. A more direct measure of the disease process is revealed by severe loss of presynaptic dopamine synthesis in the putamen and compensatory up-regulation of postsynaptic D_2-receptors in an attempt to compensate for loss of dopamine (Fig. 8A). Fig. 8B illustrates PET imaging to assess the viability of gene therapy for restoring dopamine synthesis in a monkey with an MPTP lesion in the striatum on one side of the brain. An adeno-associated virus containing the aromatic amino acid decarboxylase gene to produce the corresponding enzyme for synthesizing dopamine from L-dopa was stereotactically injected into the MPTP-injured striatum. The PET study of dopamine synthesis demonstrates that the virus has transferred the decarboxylase gene and that the enzyme has been transcribed and translated into an active state (Phelps, 2000).

Visualization of 5HT$_2$ serotonin receptor distribution and its binding ability in the human brain

Using the 5HT$_2$ serotonin receptor ligand ^{18}F-setoperone, which can cross the blood-brain barrier, it is not only possible to portray the distribution of serotonin receptors in the human brain, but also to assess how long and whether an orally administered serotonin receptor antagonist (e.g., ziprosidone) even affects the serotonin receptor (Fischman et al., 1996) (Fig. 9A).

Early diagnosis of AD

Shoghi-Jadid et al. (2002) used [^{18}F]FDDNP, a hydrophobic radiofluorinated derivative of 2-(1-[6-(dimethylamino)-2-naphthyl]ethylidene) malononitrile (DDNP), to localize and determine the load of NFTs and APs in the brains of living AD patients. Patients demonstrated greater accumulation and slower clearance of the probe in brain areas that were affected more by plaque and tangle deposition. Retention time of the tracer in brain regions known to be affected by AD is correlated with lower memory performance scores and is significantly greater in patients with AD than in control subjects (Fig. 9B).

Visualization of mRNA expression of glial fibrillary acidic protein (GFAP) using the antisense strategy

Antisense oligonucleotides are short-chain synthetic nucleic acids that bind to the corresponding sequences of the mRNA via the complementary base pairs (Zamecnik and Stephenson, 1978). Kobori et al. (1999) developed an antisense phosphorothioate oligodeoxynucleotide for mRNA of glial fibrillary acidic protein (GFAP) that was labeled with the positron emitter ^{11}C. The conjugate was administered i.v. to rats bearing glioma with high levels of GFAP mRNA. The antisense oligodeoxynucleotide (specific for GFAP mRNA) was retained in tumor cells. However, the control scrambled oligodeoxynucleotide (nonspecific for GFAP mRNA) was not retained in tumor cells.

Near-infrared optical imaging

A superficial tumor can be visualized by near-infrared optical imaging in the near-infrared range (650-900 nm) after a contrast agent containing fluorochrome is administered intravenously. This wavelength is chosen because the absorption of the light by hemoglobin and water is modest in this area and consequently the penetration depth is greater (Weissleder, 2001).

Fluorochrome-containing contrast agents, which are administered intravenously, accumulate in the tumor, which, after illumination in the near-infrared range, emits photons with higher wavelengths that can be captured by a special camera and processed as an image (Bremer et al., 2001, 2002).

There are fluorochrome contrast agents that emit photons directly after having been illuminated. These contrast agents can be bound to ligands for certain receptors, to which they then attach: for example, the ITCC (Indotricarbocyanin) was bound to the
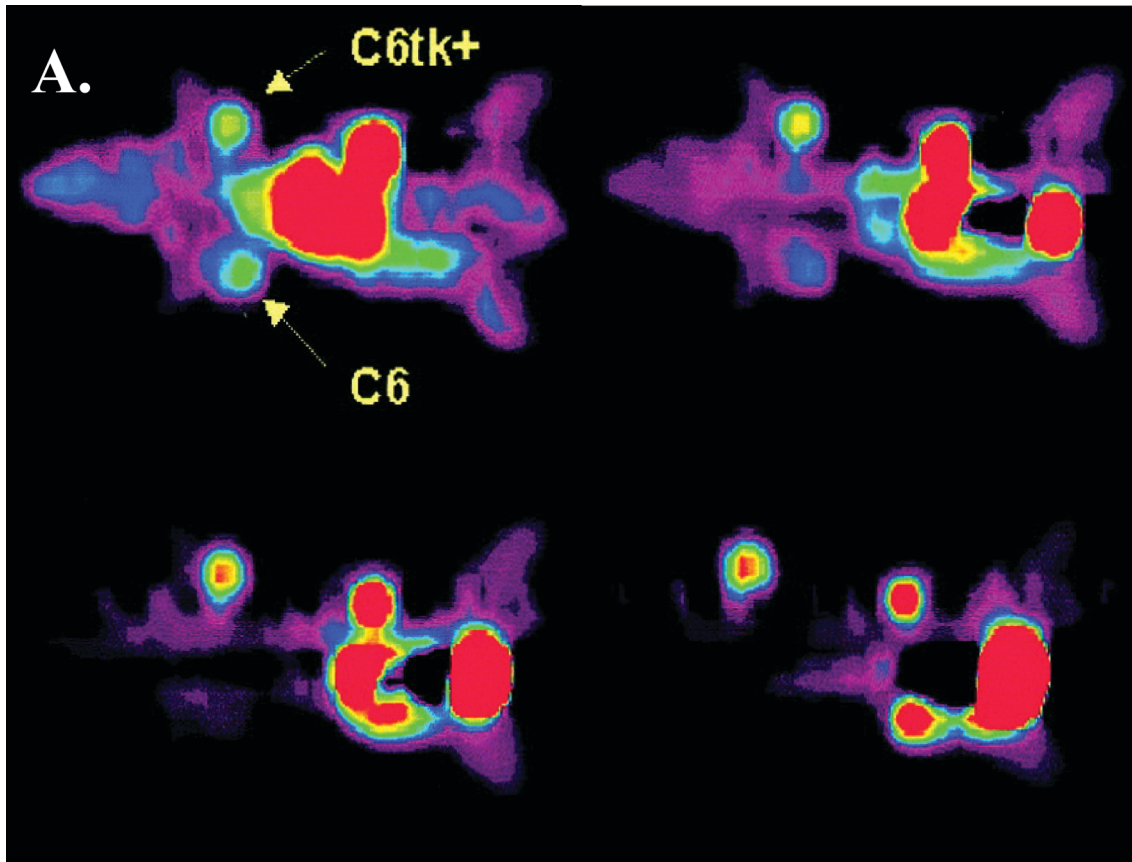
Fig. 7. A. PET images of one rat bearing a C6tk⁻ and a C6tk⁺ tumor in its flanks at 3, 20, 60 and 120 min after injection of [¹⁸F] FHPG {9-[(1-[¹⁸F] Fluoro-3-hydroxy-2-propoxy) methyl] guanine}, a substrate for viral thymidine kinase (coronal plane shown from the ventral side of the rat). Modified from Hospers et al., 2003. **B.** (FIAU)-PET (I-124-labeled 2'-fluoro-2'-deoxy-1ß-D-arabino-furanosyl-5-iodo-uracil) of a living patient. After 68 hours there was a clear difference in specific retention of iodine 124 FIAU (substrate for viral thymidine kinase) within the tumour *before* (left column) and *after* (right column, white arrow) liposome-HSV-1-tk complex transfection (vector application). Modified from Jacobs et al., 2001.
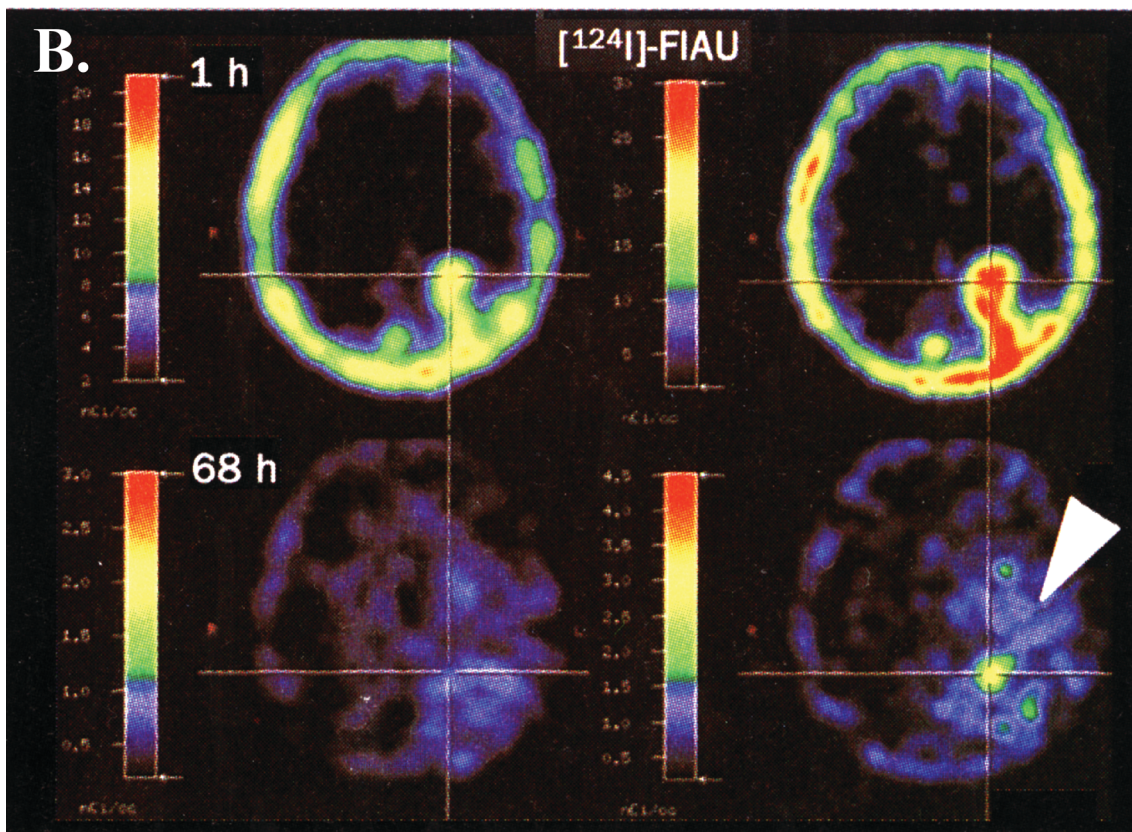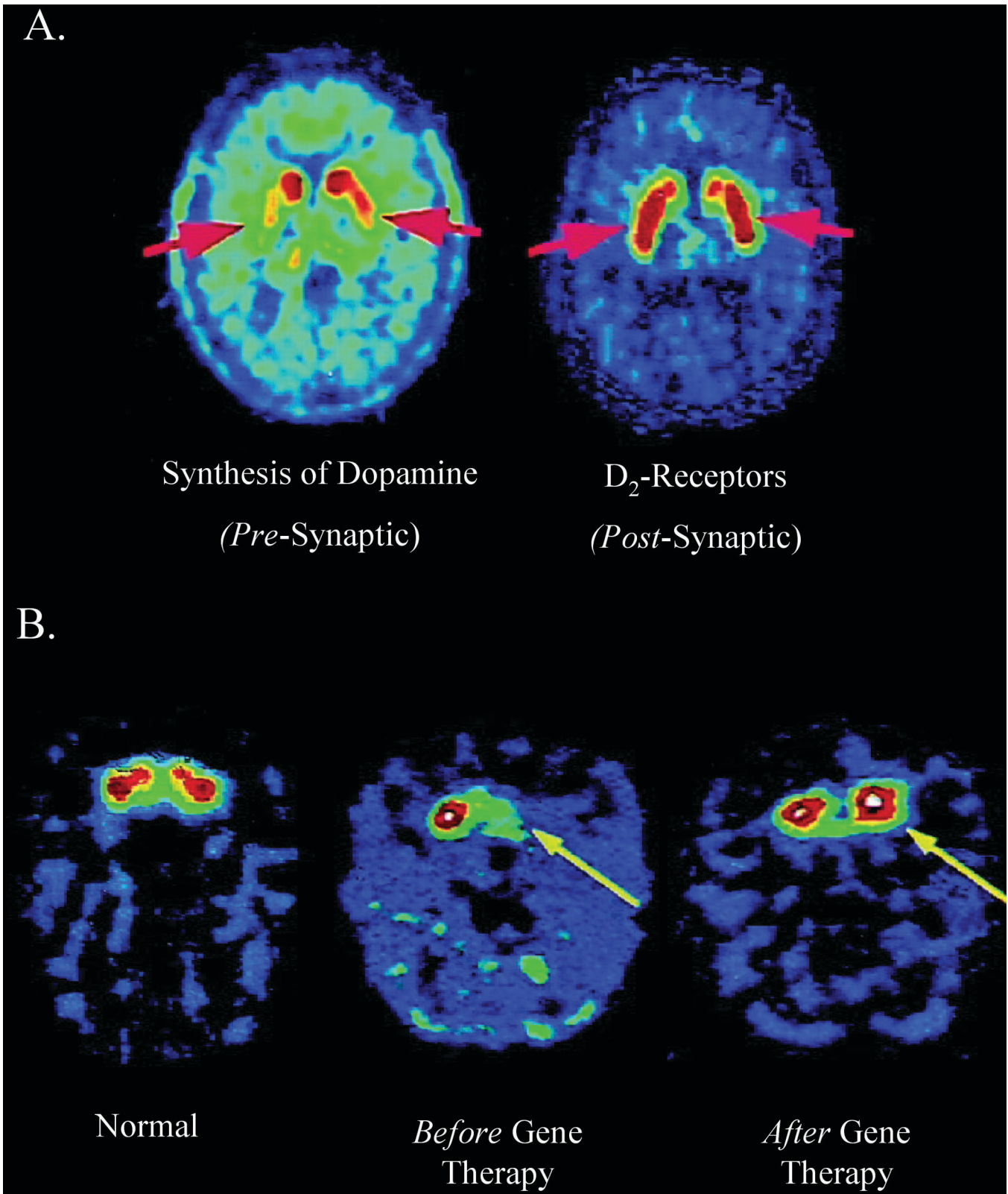
Fig. 8. A. PET images of a patient with early Parkinson's disease. Left: presynaptic synthesis of dopamine reduced by 70% (imaged with [F-18] fluorodopa) (arrows). Right: postsynaptic D_2-receptors in putamen are increased by 15% (imaged with the ligand, F-18 fluoroethylspiperone). **B.** Imaging decarboxylase gene therapy with PET in unilateral MPTP monkey model of Parkinson's disease. Dopamine synthesis was imaged with *meta*-(F-18)fluorothyrosine (substrate from aromatic amino acid decarboxylase). **Left:** Normal dopamine synthesis in caudate and putamen. **Middle:** Unilateral dopamine MPTP-induced deficit (arrow) before gene therapy. **Right:** Restoration of dopamine synthesis (arrow) after gene therapy. Modified from Phelps et al., 2000.
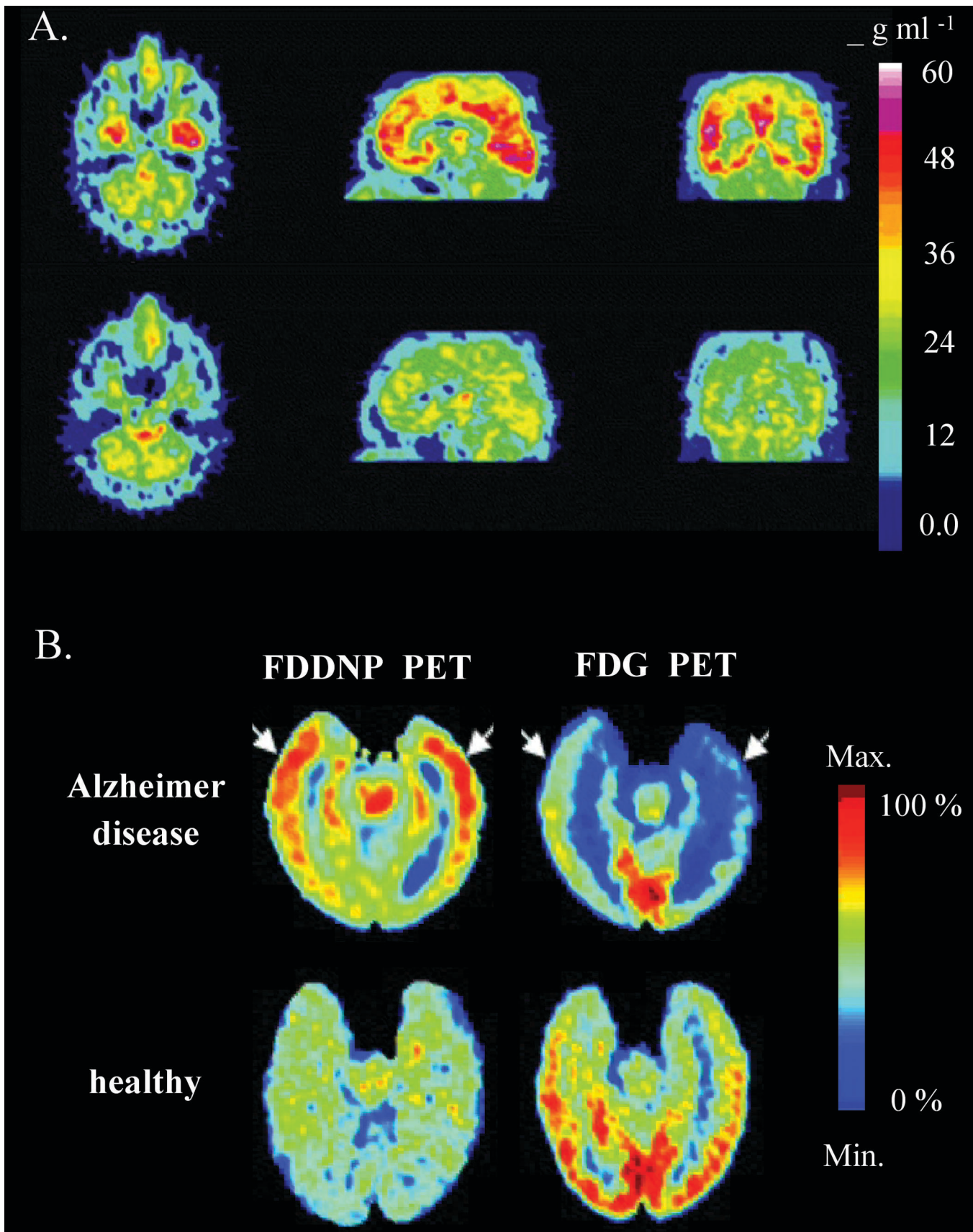
Fig. 9. A. Serotonin (5HT$_2$) receptor occupancy. Axial sagittal and coronal PET images of a healthy volunteer injected with the 5HT2 ligand 18F-setoperone before (top row) and after (bottom row) administration of 40 mg of oral ziprosidone, an antipsychotic agent with high affinity for serotonin and dopamine receptors. Modified from Fsihman et al., 1996. **B.** PET images comparing temporal lobe uptake of ^{18}F FDDNP, an amyloid-binding radiotracer, and FDG, a marker of glucose metaboslim, in a patient with AD (left upper, arrowheads), compared with those in the control subject. The patient with AD still demonstrates typical findings of decreased temporal accumulation of FDG (right upper, arrowheads). The color bar represents the scaling of the ^{18}F FDDNP and FDG images. Modified from Shoghi-Jadid et al., 2002.

somatostatin receptor ligands (Becker et al., 2001) so as to visually render tumors with a high somatostatin receptor density.

The somastotatin receptor is mainly found in ependymomas, medulloblastomas, astrocytomas, and neuroendocrine tumors (Guyotat et al., 2001, 2001a; Papos et al., 2001). Apoptotic cells express phosphatidylserine, a membrane phospholipid on the cell surface (normally in the inner cell membrane).

Petrovsky et al. (2003) demonstrated that active Cy annexin [annexin V labeled with the fluorophore Cy5.5 (Cy)] can be used as a near-infrared optical imaging probe to image phosphatidylserine, and hence apoptosis, from outside an intact living animal (the 9L gliosarcoma model) .

There are also fluorochrome contrast agents that do not emit photons immediately during illumination in the near-infrared range because they first have to be activated by proteases (Weissleder et al., 1999, Bremer et al., 2001, 2002) (Fig. 10). These proteases (e.g., matrix-metalloproteinases, cathepsin) -- so to speak -- mill a path for the tumor through the tissue and make infiltration possible (Koblinski et al., 2000). Since higher amounts of proteases are formed in tumors, the contrast agent is activated most there.

In malignant gliomas *matrix-metalloproteinases* play an important role in angiogenesis (Wild-Bode et al., 2001). Substances that inhibit matrix-metalloproteinases are used to inhibit angiogenesis (Bremer et al., 2001).

This therapy can be followed in superficial tumors by near-infrared optical imaging. If the matrix-metalloproteinase is inactivated by the angiogenesis inhibitor AG 3340 (Prinomastat), the fluorochrome contrast agents are ineffective. The tumor is therefore not visible in the near-infrared image. Recently the apoptosis enzyme caspase 3 and its inhibitor were identified in cell cultures in vitro by near-infrared light (Weissleder and Mahmood, 2001).

With conventional near-infrared optical imaging, however, the resolution is significantly worse than that of scintigraphy, PET, or even MRI. Moreover, the penetration depth is only 1-2 cm (intraoperative or endoscopic use is feasible here). Thanks to the development of very specific contrast agents (matrix-metalloproteinases) and new technologies with greater penetration depths (up to 10 cm), however, it is gaining increasingly in significance (Mahmood et al., 1999; Weissleder, 2001; Weissleder and Mahmood, 2001; Ntziachristos et al., 2002, 2003; Weissleder and Ntziachristos, 2003).

One such newly developed volumetric imaging technique (fluorescence molecular tomography, FMT) collects photons that have propagated through tissue at multiple projections and combines these measurements tomographically to assess the distribution of fluorochromes in deep tissues (it is possible to quantify pico- to femtomole quantities of fluorochromes) (Ntziachristos et al., 2002, 2003). With this method cathepsin B activity could be measured in 9L

gliosarcomas which were stereotactically implanted into unilateral brain hemispheres of nude mice (Fig. 11).

Scintigraphy

Tumor localization (receptor scintigraphy)

Tumor scintigraphy involves the intravenous administration of a radiopharmaceutical that localizes in certain tumor tissues for subsequent imaging and computer acquisition of data. This standard is limited to gamma camera imaging.

Tumor cells express significantly higher numbers of VEGF receptors than normal non-neoplastic tissues. Therefore, (^{123})I-VEGF(165) may be a potentially useful tracer for in vivo imaging of meningiomas (Li et al., 2001). [Indium-111-DTPA-Arg1] Substance P can be used successfully to visualize substance P receptors in rat brain cortex membranes in vivo by gamma camera scintigraphy (Breeman et al., 1996). There also seems to be a promising role of Tc-99m-sestamibi scintigraphy (transport substrate for P-glycoprotein-related multidrug resistance) in the staging and prognosis of the therapeutic response of stage IV neuroblastoma (Burak et al., 1999). Somatostatin receptors in ependymomas, medulloblastomas, astrocytomas, ectomesenchymomas, and neuroendocrine tumors can be visualized by (^{125})I Octreotat (Octreoscan) (Guyotat et al., 2001a,b; Papos et al., 2001).

This allows for a more precise assessment of therapy with the somatostatin analogue Octreotat in humans, since the density of the somatostatin receptors decreases if there is a response to therapy (Papos et al., 2001).

Apoptotic cells express phosphatidylserine, a membrane phospholipid (usually inside the cell membrane) on the cell surface . This can be visually rendered with radiolabeled ^{99}mTC Annexin (endogenous human protein). Annexin is retained sixfold more strongly in apoptotic tissue. The VIP (vasointestinal peptide) receptor can be visually rendered in neuroendocrine tumors and their metastases (liver) in humans by (^{123})I-VIP (Hessenius et al., 2000).

Autoradiography

By autoradiography, we mean the detection of radiolabeled molecules on X-rays. Gene expression in vivo can be autoradiographically quantitated with *antisense radiopharmaceutical*s.

Antisense oligonucleotides are short-chain synthetic nucleic acids, which are connected by complementary base pairs to corresponding sequences of mRNA. To make the antisense oligonucleotides more resistant to enzymes, they were chemically modified [oligonucleotide derivatives = peptide nucleic acid (PNA)] (Nielsen et al., 1991).

Shi et al. (2000) developed an antisense imaging agent comprising of an iodinated peptide nucleic acid (PNA) conjugated to a monoclonal antibody to the rat
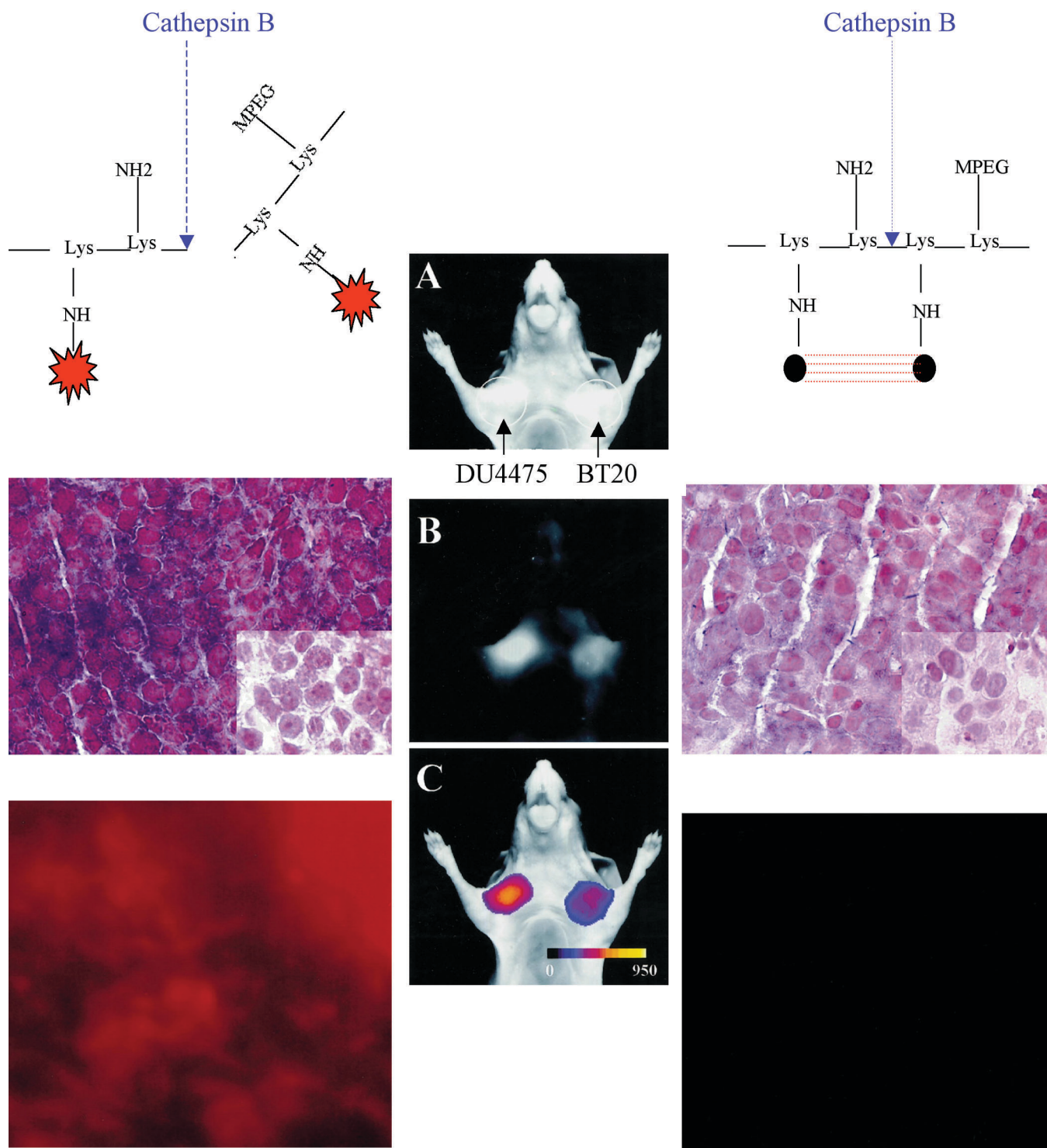
Fig. 10. Center: Mouse with the highly invasive breast adenocarcinoma (DU4475) implanted on the right of the chest and the *well differentiated* adenocarcinoma (BT20) on the left, 24 hous after intravenous injection of the cathepsin-B-sensitive autoquenched probe. **A.** Light image. **B.** Raw NIRF image **C.** Color-encoded NIRF signal (arbitrary units of NIRF intensity) superimposed on light image. Note the higher fluorescent signal depicted on the highly invasive breast leasion. **Left and right top images:** Proteolytic activation of fluorochrome contrast agent via a protease (cathepsin B). Inactive contrast agent before (right) (no photon emission, but emission of heat) and after (left) action of cathepsin B (photon emission in near-infrared). MPEG: Methoxypolyethylenglycol for stabilization and biocompatibility. **Left and right middle images:** Photomicrograph of cathepsin-B-expression in DU4775 tumor (left) compared with the well-differentiated adenocarcinoma (right). **left and right bottom images:** NIRF microscopy of unstained frozen tumor sections. x 40. The cathepsin B-generated fluorescence signal is higher in the highly invasive DU 4475 tumor (left) than in the well-differentiated BT20 adenocarcinoma (right). Modified from Bremer et al., 2002.

transferrin receptor (highly expressed at the blood-brain barrier) by using avidin-biotin technology. The PNA was an antisense to the sequence around the methionine initiation codon of the luciferase mRNA. The [(125)I] PNA conjugate was injected intravenously in animals with C6 rat gliomas which were permanently transfected with a luciferase expression plasmid. The expression of the luciferase transgene in the tumors in vivo was confirmed by the measurement of luciferase enzyme activity in the tumor extract and corresponded to the autoradiographic brain scans (Fig. 12). Additionally, with antisense radiopharmaceuticals the expression of the huntington gene of Huntington's disease (HD) could be quantified in vivo (Lee et al., 200a,b) and the Abeta amyloid burden could be visualized in the brain of transgenic mice with Alzheimer`s disease in vivo [(^{125})I-Abeta(1-40)-8D3] (Lee et al., 2002a,b).

Molecular imaging outside of the central nervous system

Carcinoembryonic antigen (CEA) can be visualized scintigraphically and is presently used for detecting colon cancer recurrence in patients (Libutti et al., 2001). The autoimmune destruction of beta cells in the pancreatic islets of mice (Type 1 diabetes) can be determined at an early stage by lymphocytes labeled with MIONs (Moore et al., 2002).

Gene therapy of liver cell carcinoma in rats (NaI-Symporter-Gene) can be followed scintigraphically by the uptake of ^{125}I (Haberkorn et al., 2001). Bombesin receptor scintigraphy is being tested in breast, prostate, and small-cell lung cancer (Scopinaro et al., 2002; de Vincentis et al. 2002). With the help of antisense gadolinium conjugates it is still possible to visualize prostate cancer intracellularly in rats using MRI (Heckl et al. 2003).

In future applications prostate carcinoma in humans could also be localized with near- infrared light with activatable contrast agent due to the high expression of prostate-specific antigen (serine protease) (Tung et al., 2000).

Since thrombin is also a serine protease, thrombosis could also be detected at an early stage by activatable
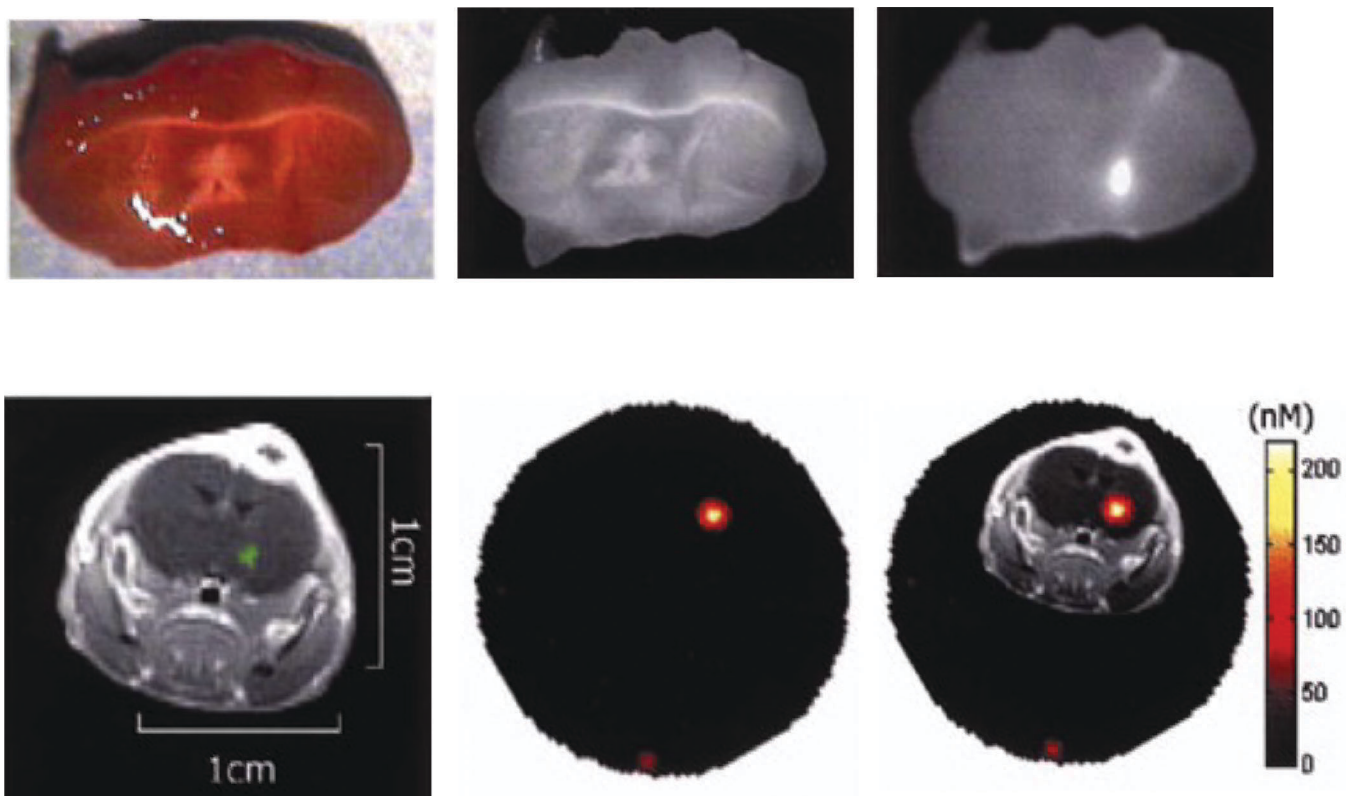

Fig. 11. Top row: left: Axial brain section through the 9L tumor imaged with white light. **Middle.** Axial brain section through the 9L tumor imaged with monochromatic light at the excitation wavelength (675 nm). **Right**: Fluorescence image of the same axial brain section demonstrating a marked fluorescent probe activation, congruent with the tumor position identified by gadolinium-enhanced MRI and FMT. **botton row: Left:** Axial MR slice [(T1-weighted spin-echo sequence (TR:TE, 300:13 msec)] of a nude mouse brain implanted with a 9L gliosarcoma, which is shown in green after gadolinium enhancement. **Middle:** FMT slice obtained from the volume of interest. **Right**: Superposition of the MR axial slice passing through the tumor **(a)** onto the corresponding FMT slice after appropriately translating the MR image to the actual dimensions of the FMT image. Modified from Ntziachristos et al., 2003.
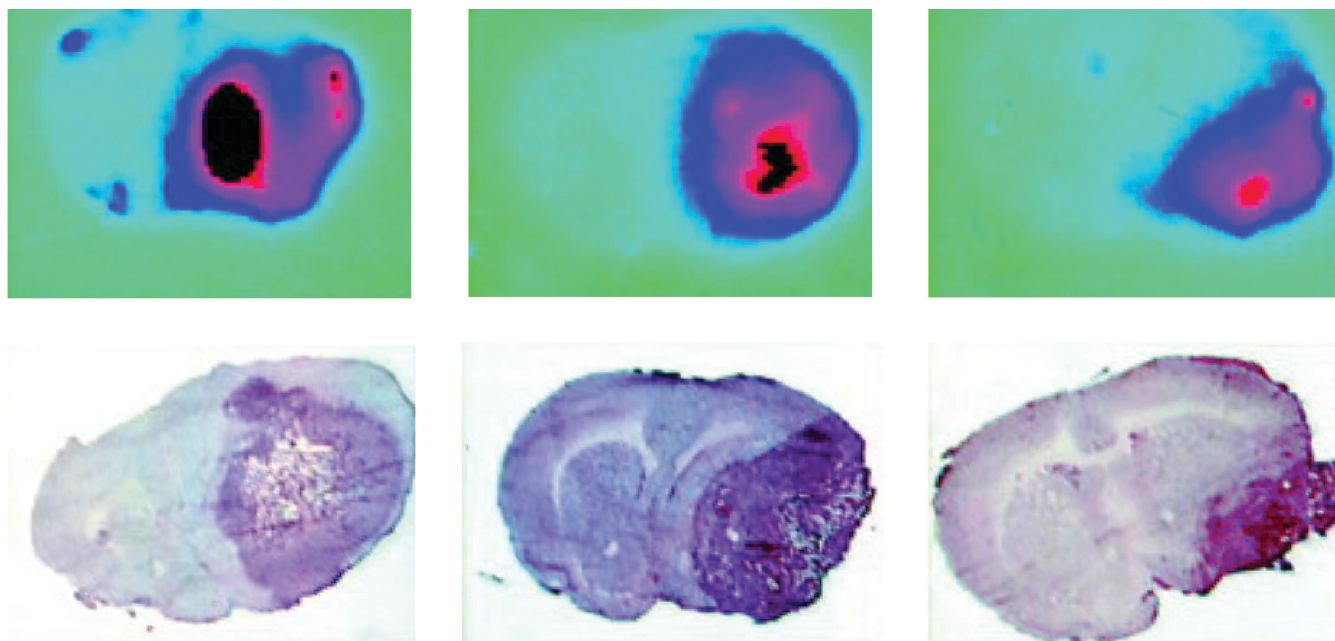
Fig. 12. The size of the C6-glioma transfected with the luciferase gene imaged with the antisense radiopharmaceutical was comparable to the size of the tumor shown on the autopsy stain. Modified from Shi et al., 2000.

contrast agents in the near-infrared light (Jaffer et al., 2002; Tung et al., 2002). The glycoprotein IIb/IIIa receptor can be shown scintigraphically by activated thrombocytes. This makes it possible to diagnose deep-vein thrombosis (Bates et al., 2003).

Chen et al. (2002) showed that cathepsin B activity in atherosclerotic lesions can be imaged in vivo by using near-infrared optical imaging. The same method can be used to distinguish polyps from healthy intestinal tissue in adenomatous polyposis in rats (Marten et al., 2002).

Folate receptor-positive nasopharyngeal epidermoid carcinoma can be detected by a novel near-infrared folate receptor (FR)-targeted imaging probe (Moon et al., 2003). The creation of new vessels in the tumor can be portrayed in animal experiments by specific markers of angiogenesis with MRI (Sipkins et al., 1998; Anderson et al., 2000).

In humans antiangiogenic therapy with the antibody ^{99m}Tc Vitaxin against the vitronectin receptor (alpha (v) beta (3) Integrin) is already being monitored scintigraphically (Posey et al., 2001). It would be helpful to be able to determine HER-2 levels by MRI for planning therapy with herceptin in metastasizing breast carcinoma (to date this has been done in mice) (Artemov et al., 2003).

Finally (111)In-DTPA-folate is being clinically tested to see whether malignant and benign ovarian masses can be scintigraphically distinguished, depending on different expression levels of cell-membrane folate receptor (Siegel et al., 2003).

Concluding remarks

Molecular imaging is still largely in the animal experimental phase. Through further research activity, mostly with regard to safe application in humans, it will probably play a crucial role in detecting lesions based upon their molecular signatures, in characterizing lesions in situ to aid in treatment decisions, and in helping define successful therapeutic drug levels on an individual basis. Thus, molecular imaging represents a useful non-invasive supplement to histological approaches.

References

Adachi M., Sampath J., Lan L.B., Sun D., Hargrove P., Flatley R.M., Tatum A., Ziegelmeier M.Z., Wezeman M., Matherly L.H., Drake R.R. and Schuetz J.D. (2002). Expression of MRP4 confers resistance to ganciclovir and compromises bystander cell killing. J. Biol. Chem. 11, 277, 38998-9004.

Anderson S.A., Rader R.K., Westlin W.F., Null C., Jackson D., Lanza G.M., Wickline S.A. and Kotyk J.J. (2000). Magnetic resonance contrast enhancement of neovasculature with alpha (v) beta (3)-targeted nanoparticles. Magn. Reson. Med. 44, 433-439.

Artemov D., Mori N., Ravi R. and Bhujwalla Z.M. (2003). Magnetic Resonance Molecular Imaging of the HER-2/neu Receptor. Cancer Res. 63, 2723-2727.

Bates S.M., Lister-James J., Julian J.A., Taillefer R., Moyer B.R. and Ginsberg J.S. (2003). Imaging characteristics of a novel technetium Tc 99m-labeled platelet glycoprotein IIb/IIIa receptor antagonist in

patients with acute deep vein thrombosis or a history of deep vein thrombosis. Arch. Intern. Med. 24, 63, 452-456.

Becker A., Hessenius C., Licha K., Ebert B., Sukowski U., Semmler W., Wiedenmann B. and Grötzinger C. (2001). Receptor-targeted optical imaging of tumors with near-infrared fluorescent ligands. Nat. Biotechnol. 19: 327-331.

Benveniste H., Einstein G., Kim K.R., Hulette C and Johnson A. (1999). Detection of neuritic plaques in Alzheimer`s disease by magnetic resonance microscopy. Proc. Natl. Acad. Sci. USA 96, 14079-14084.

Breeman W.A., VanHagen M.P., Visser-Wisselaar H.A., van der Pluijm M.E., Koper J.W., Setyono-Han B., Bakker W.H., Kwekkeboom D.J., Hazenberg M.P., Lamberts S.W., Visser T.J. and Krenning E.P. (1996). In vitro and in vivo studies of substance P receptor expression in rats with the new analog [indium-111-DTPA-Arg1]substance P. J. Nucl. Med. 37,108-117.

Bremer C., Tung C.H. and Weissleder R. (2001). In vivo molecular target assessment of matrix metalloproteinase inhibition. Nat. Med. 7, 743-748.

Bremer C., Tung C.H., Bogdanov A. Jr. and Weissleder R. (2002). Imaging of differential protease expression in breast cancers for detection of aggressive tumor phenotypes. Radiology 222, 814-81.

Bulte J.W., Zhang S., van Gelderen P., Herynek V., Jordan E.K., Duncan I.D. and Frank J.A. (1999). Neurotransplantation of magnetically labeled oligodendrocyte progenitors: magnetic resonance tracking of cell migration and myelination. Proc. Natl. Acad. Sci. USA 21, 96, 15256-15261.

Bulte J.W., Ben-Hur T., Miller B.R., Mizrachi-Kol R., Einstein O., Reinhartz E., Zywicke H.A., Douglas T. and Frank J.A. (2003). MR microscopy of magnetically labeled neurospheres transplanted into the Lewis EAE rat brain. Magn. Reson. Med. 50, 201-5.

Burak Z., Yuksel D.A., Cetingul N., Kantar M., Ozkilic H. and Moretti J.L. (1999). The role of 99Tcm-sestamibi scintigraphy in the staging and prediction of the therapeutic response of stage IV neuroblastoma: comparison with 131I-MIBG and 99Tcm-MDP scintigraphy.Nucl. Med. Commun. 20, 991-1000.

Chen J., Tung C.H., Mahmood U., Ntziachristos V., Gyurko R., Fishman M.C., Huang P.L. and Weissleder R. (2002). In vivo imaging of proteolytic activity in atherosclerosis. Circulation 11, 2766-2771.

De Vincentis G., Scopinaro F., Varvarigou A,. Ussof W., Schillaci O., Archimandritis S, Corleto V., Longo F. and Delle Fave G. (2002). Phase I trial of technetium [Leu13] bombesin as cancer seeking agent: possible scintigraphic guide for surgery? Tumori 88, S28-30.

Enochs W.S., Petherick P., Bogdanova A., Mohr U. and Weissleder R. (1997). Paramagnetic metal scavenging by melanin: MR imaging. Radiology 204, 417-23.

Fischman A.J., Bonab A.A., Babich J.W., Alpert N.M., Rauch S.L., Elmaleh D.R., Shoup T.M., Williams S.A. and Rubin R.H. (1996). Positron emission tomographic analysis of central 5-hydroxytryptamine2 receptor occupancy in healthy volunteers treated with the novel antipsychotic agent, ziprasidone. J. Pharmacol. Exp. Ther. 279, 939-47.

Fleige G., Nolte C., Synowitz M., Seeberger F., Kettenmann H. and Zimmer C. (2001). Magnetic labeling of activated microglia in experimental gliomas. Neoplasia 3, 489-499.

Guyotat J., Champier J., Jouvet A., Signorelli F., Houzard C., Bret P., Saint Pierre G. and Fevre Montagne M. (2001a). Differential expression of somatostatin receptors in ependymoma: Implications for diagnosis. Int. J. Cancer 95, 144-151.

Guyotat J., Champier J., Pierre G.S., Jouvet A., Bret P., Brisson C., Belin M.F., Signorelli F. and Montagne M.F. (2001a). Differential expression of somatostatin receptors in medulloblastoma. J. Neurooncol. 51, 93-103.

Haberkorn U., Henze M., Altmann A., Jiang S., Morr I., Mahmut M., Peschke P., Kubler W., Debus J. and Eisenhut M. (2001b). Transfer of the human NaI symporter gene enhances iodide uptake in hepatoma cells. J. Nucl. Med. 42, 317-325.

Heckl S., Debus J., Jenne J., Pipkorn R., Waldeck W., Spring H., Rastert R., von der Lieth C.W. and Braun K. (2002). CNN-Gd3+ enables cell nucleus molecular imaging of prostate cancer cells: the last 600 nm. Cancer Res. 62, 7018-24.

Heckl S. Pipkorn R., Waldeck W., Spring H., Jenne J., von der Lieth C.W., Corban-Wilhelm H., Debus J. and Braun K. (2003). Intracellular visualization of prostate cancer using magnetic resonance imaging. Cancer Res. 63, 4766-4772.

Hessenius C., Bäder M., Meinhold H., Böhmig M., Faiss S., Reubi J.C. and Wiedenmann B. (2000). Vasoactive intestinal peptide receptor scintigraphy in patients with pancreatic adenocarcinomas or neuroendocrine tumours. Eur. J. Nucl. Med. 27, 1684-1693.

Högemann D., Josephson L., Weissleder R. and Basilion J.P. (2000). Improvement of MRI probes to allow efficient detection of gene expression. Bioconjug. Chem. 11, 941-946.

Högemann D., Ntziachristos V., Josephson L. and Weissleder R. (2002). High throughput magnetic resonance imaging for evaluating targeted nanoparticle probes. Bioconjug. Chem. 13, 116-121.

Hospers G.A., Calogero A., van Waarde A., Doze P., Vaalburg W., Mulder N.H. and de Vries E.F. (2000). Monitoring of Herpes Simplex Virus Thymidine Kinase Enzyme Activity Using Positron Emission Tomography. Cancer Res. 60, 1488-1491.

Ichikawa T., Hogemann D., Saeki Y., Tyminski E., Terada K., Weissleder R., Chiocca E.A. and Basilion J.P. (2002). MRI of transgene expression: correlation to therapeutic gene expression. Neoplasia 4, 523-30.

Jacobs A., Voges J., Reszka R., Lercher M., Gossmann A., Kracht L., Kaestle C., Wagner R., Wienhard K. and Heiss W.D. (2001). Positron-emission tomography of vector-mediated gene expression in gene therapy for gliomas. Lancet 358, 727-9.

Jaffer F.A., Tung C.H., Gerszten R.E. and Weissleder R. (2002). In vivo imaging of thrombin activity in experimental thrombi with thrombin-sensitive near-infrared molecular probe. Arterioscler. Thromb. Vasc. Biol. 22, 1929-1935.

Josephson K., Tung C., Melder R., Moore A. and Weissleder R. (1999). High efficiency magnetic cell labeling through Tat peptides. Bioconjug. Chem.10, 186-191.

Koblinski J.E., Ahram M. and Sloane B.F. (2000). Unraveling the role of proteases in cancer. Clinica Chimica Acta 291, 113-135.

Kobori N., Imahori Y., Mineura K., Ueda S. and Fujii R. (1999). Visualization of mRNA expression in CNS using 11C-labeled phosphorothioate oligo-deoxynucleotide. Neuroreport 10, 2971-2974.

Lee H.J., Boado R.J., Braasch D.A., Corey D.R. and Pardridge W.M. (2002). Imaging gene expression in the brain in vivo in a transgenic mouse model of Huntington's disease with an antisense radiopharmaceutical and drug-targeting technology. J. Nucl. Med. 43, 948-956.

Lee H.J., Zhang Y., Zhu C., Duff K. and Pardridge W.M. (2002a). Imaging brain amyloid of Alzheimer disease in vivo in transgenic mice with an Abeta peptide radiopharmaceutical. J. Cereb. Blood

Flow Metab. 22, 223-31.

Lewin M., Carlessso N., Tung C.H., Cory D., Scadden D.T. and Weissleder R. (2000). Tat peptide-derivatized magnetic nanoparticles allow in vivo tracking and recovery of progenitor cells. Nat. Biotechnol. 18, 410-414.

Li S., Peck-Radosavljevic M., Koller E., Koller F., Kaserer K., Kreil A., Kapiotis S., Hamwi A., Weich H.A., Valent P., Angelberger P., Dudczak R. and Virgolini I. (2001). Characterization of (123)I-vascular endothelial growth factor-binding sites expressed on human tumour cells: possible implication for tumour scintigraphy. Int. J. Cancer 91, 789-796.

Libutti S.K., Alexander H.R. Jr., Choyke P., Bartlett D.L., Bacharach S.L., Whatley M., Jousse F., Eckelman W.C., Kranda K., Neumann R.D. and Carrasquillo J.A. (2001). A prospective study of 2-[18F] fluoro-2-deoxy-D-glucose/positron emission tomography scan, 99mTc-labeled arcitumomab (CEA-scan), and blind second-look laparotomy for detecting colon cancer recurrence in patients with increasing carcinoembryonic antigen levels. Ann. Surg. Oncol. 8, 779-86.

Louie A.Y., Hüber M.M., Ahrens E.T., Rothbächer U., Moats R., Jacobs R.E., Fraser S.E. and Meade T.J. (2000). In vivo visualisation of gene expression using magnetic resonance imaging. Nat. Biotechnol. 18, 321-325.

Lovell M.A., Robertson J.D., Teesdale W.J., Campbell J.L. and Markesbery W.R. (1998). Copper, iron, and zinc in Alzheimer`s disease senile plaques. J. Neurol. Sci. 158, 47-52.

Mahmood U., Tung C.H., Bogdanov A. and Weissleder R. (1999). Near-infrared optical imaging of protease activity for tumor detection. Radiology 213, 866-870.

Marten K., Bremer C., Khazaie K., Sameni M., Sloane B., Tung C.H. and Weissleder R. (2002). Detection of dysplastic intestinal adenomas using enzyme-sensing molecular beacons in mice. Gastroenterology 122, 406-414.

Moon W.K., Lin Y., O'Loughlin T., Tang Y., Kim D.E., Weissleder R. and Tung C.H. (2003). Enhanced tumor detection using a folate receptor-targeted near-infrared fluorochrome conjugate. Bioconjug. Chem.14, 539-545.

Moore A., Zhe Sun P., Cory D., Högemann D., Weissleder R. and Lipes M.A. (2002). MRI of insulitis in autoimmune diabetes. Magn. Reson. Med. 47, 751-758.

Nicholas T.W., Read S.B., Burrows F.J. and Kruse C.A. (2003). Suicide gene therapy with Herpes simplex virus thymidine kinase and ganciclovir is enhanced with connexins to improve gap junctions and bystander effects. Histol. Histopathol. 18, 495-507.

Nielsen P.E., Egholm M., Berg R.H. and Buchardt O. (1991). Sequence-selective recognition of DNA by strand displacement with a thymine-substituted polyamide. Science 254, 1497-1500.

Ntziachristos V., Tung C.H., Bremer C. and Weissleder R. (2002). Fluorescence molecular tomography resolves protease activity in vivo. Nat. Med. 8, 757-60.

Ntziachristos V., Bremer C. and Weissleder R. (2003). Fluorescence imaging with near-infrared light: new technological advances that enable in vivo molecular imaging. Eur. Radiol. 13, 195-208.

Papos M., Pekrun A., Herms J.W., Behr T.M., Meller J., Rustenbeck H.H., Kretzschmar H.A. and Becker W. (2001). Somatostatin receptor scintigraphy in the management of cerebral malignant ecto-mesenchymoma: a case report. Pediatr. Radiol. 31, 169-172.

Petrovsky A., Schellenberger E., Josephson L., Weissleder R. and Bogdanov A. Jr. (2003). Near-infrared fluorescent imaging of tumor apoptosis. Cancer Res. 15, 63,1936-42.

Phelps M.E. (2000). Inaugural article: positron emission tomography provides molecular imaging of biological processes.Proc. Natl. Acad. Sci. USA 1, 97, 9226-9233.

Poduslo J.F., Wegenack T.M., Curran G.L., Wisniewski T., Sigurdsson E.M., Macura S.I., Borowski B.J. and Jack C.R. Jr. (2002). Molecular targeting of Alzheimer's amyloid plaques for contrast-enhanced magnetic resonance imaging. Neurobiol. Dis. 11, 315-29.

Posey J.A., Khazaeli M.B., Del Grosso A., Saleh M.N., Lin C.Y., Huse W. and LoBuglio A.F. (2001). A pilot trial of Vitaxin, a humanized anti-vitronectin receptor [anti alpha (v) beta (3)] antibody in patients with metastatic cancer. Cancer Biother. Radiopharm. 16, 125-32.

Rainov N.G. (2000). A phase III clinical evaluation of herpes simplex virus type 1 thymidine kinase and ganciclovir gene therapy as an adjuvant to surgical resection and radiation in adults with previously untreated glioblastoma multiforme. Hum. Gene Ther. 11, 2389-2401.

Scopinaro F., Varvarigou A.D., Ussof W., De Vincentis G., Sourlingas T.G., Evangelatos G.P., Datsteris J. And Archimandritis S.C. (2002). Technetium labeled bombesin-like peptide: preliminary report on breast cancer uptake in patients..Cancer Biother. Radiopharm. 17, 327-35.

Shen T., Weissleder R., Papisov M., Bogdanov A. Jr. and Brady T.J. (1993). Monocrystalline iron oxide nanocompounds (MION): physico-chemical properties. Magn. Reson. Med. 29, 599-604.

Shi N., Boado R.J. and Pardridge W.M. (2000). Antisense imaging of gene expression in the brain in vivo. Proc. Natl. Acad. Sci. USA 97, 14709-14714.

Shoghi-Jadid K., Small G.W., Agdeppa E.D., Kepe V., Ercoli L.M., Siddarth P., Read S., Satyamurthy N., Petric A., Huang S.C. and Barrio J.R. (2002). Localization of neurofibrillary tangles and beta-amyloid plaques in the brains of living patients with Alzheimer disease. Am. J. Geriatr. Psychiatry 10, 24-35.

Siegel B.A., Dehdashti F., Mutch D.G., Podoloff D.A., Wendt R., Sutton G.P., Burt R.W., Ellis P.R., Mathias C.J., Green M.A. and Gershenson D.M. (2003). Evaluation of (111) In-DTPA-Folate as a Receptor-Targeted Diagnostic Agent for Ovarian Cancer: Initial Clinical Results. J. Nucl. Med. 44, 700-707.

Sipkins D.A., Cheresh D.A., Kazemi M.R., Nevin L.M., Bednarski M.D. and Li K.C. (1998). Detection of tumor angiogenesis in vivo by alpha (V) beta (3)-targeted magnetic resonance imaging. Nat. Med. 4, 623-626.

Tung C.H., Mahmood U., Bredow S. and Weissleder R. (2000). In vivo imaging of proteolytic enzyme activity using a novel molecular reporter. Cancer Res. 60, 4953-4958.

Tung C.H., Gerszten R.E., Jaffer F.A. and Weissleder R. (2002). A novel near-infrared fluorescence sensor for detection of thrombin activation in blood. Chembiochem. 3, 207-211.

Weissleder R. (2001). A clearer vision for in vivo imaging. Nat. Biotechnol. 19, 316-317.

Weissleder R. and Mahmood U. (2001). Molecular imaging. Radiology 19, 316-333.

Weissleder R. and Ntziachristos V. (2003). Shedding light onto live molecular targets. Nat. Med. 9, 123-128.

Weissleder R., Simonova M., Bogdanova A., Bredow S., Enochs W.S. and Bogdanov A. Jr. (1997). MR imaging and scintigraphy of gene expression through melanin induction. Radiology 204, 417-423.

Weissleder R., Tung C.H., Mahmood U. and Bogdanov A. Jr. (1999). In vivo imaging of tumors with protease-activated near-infrared fluorescent probes. Nat. Biotechnol. 17, 375-378.

Weissleder R., Moore A., Mahmood U., Bhorade R., Benveniste H., Chiocco E.A. and Basilion J.P. (2000). In vivo magnetic resonance imaging of transgene expression. Nat. Med. 6, 351-354.

Wild-Bode C., Weller M., Rimner A., Dichgans J. and Wick W. (2001). Sublethal irradiation promotes migration and invasiveness of glioma cells: implications for radiotherapy of human glioblastoma. Cancer Res. 61, 2744-2750.

Zamecnik P.C. and Stephenson M.L. (1978). Inhibition of Rous sarcoma by virus replication and cell transformation by a specific oligodeoxynucleotide. Proc. Natl. Acad. Sci. USA 75, 280-284.

Zhang Z.G., Jiang Q., Zhang R., Zhang L., Wang L., Zhang L., Arniego P., Ho K.L. and Chopp M. (2003). Magnetic resonance imaging and neurosphere therapy of stroke in rat. Ann. Neurol. 53, 259-263.